pubs.acs.org/Biomac

Article

Systematic Evaluation of Macromolecular Carbohydrate-Lectin Recognition Using Precision Glycopolymers

Cole A. Williams,[‖] Daniel J. Stone,[‖] Soumil Y. Joshi, Gokhan Yilmaz, Parisa Farzeen, Sungjin Jeon, Zamira Harris-Ryden, C. Remzi Becer, Sanket A. Deshmukh, and Cassandra E. Callmann*

Cite This: *Biomacromolecules* 2024, 25, 7985−7994

Read Online

ACCESS | Metrics & More | Article Recommendations | Supporting Information

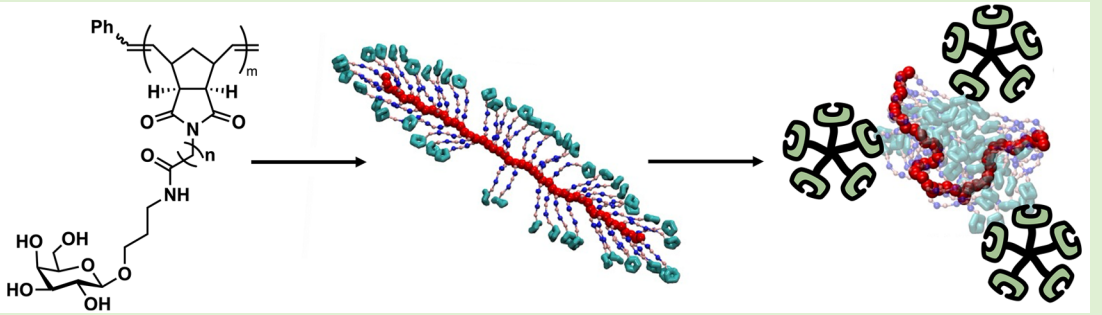

ABSTRACT: The precise modulation of protein-carbohydrate interactions is critical in glycobiology, where multivalent binding governs key cellular processes. As such, synthetic glycopolymers are useful for probing these interactions. Herein, we developed precision glycopolymers (PGPs) with unambiguous local chemical composition and well-defined global structure and systematically evaluated the effect of polymer length, hydrophobicity, and backbone hybridization as well as glycan density and identity on the binding to both mammalian and plant lectins. Our studies identified glycan density as a critical factor, with PGPs below 50% grafting density showing significantly weaker lectin interactions. Coarse-grained molecular dynamics simulations suggest that the observed phenomena may be due to a decrease in carbohydrate-carbohydrate interactions in fully grafted PGPs, leading to improved solvent accessibility. In functional assays, these PGPs reduced the cell viability and migration in 4T1 breast cancer cells. Our findings establish a structure−activity relationship in glycopolymers, providing new strategies for designing synthetic glycomacromolecules for a myriad of applications.

INTRODUCTION

Nature has evolved carbohydrates as effectors of key biological processes, including molecular recognition, intercellular communication, cellular adhesion, and signal transduction.[1,2] As such, there is broad interest in the fields of chemistry, materials science, and chemical biology in understanding the molecular basis for this complex communication.[3,4] Moreover, synthetic glycomaterials that can probe and manipulate biological processes hold significant importance in both biotechnological[5−10] and biomedical[11−18] contexts.

Strikingly, the entire mammalian glycome is comprised of only ∼10 different monosaccharides.[19,20] Thus, the complex, multifunctional role of carbohydrates relies not only on their chemical composition but also on their macromolecular presentation on scaffold proteins and lipids, coupled with their supramolecular assembly and structural ensemble with other glycoconjugates.[19,21] In the body, carbohydrates are presented as dense side chains on polypeptide backbones, forming natural "bottlebrush" polymers on proteins and cell surfaces.[22,23] This high density display leads to tight binding to their protein (lectin) binding partners ($K_d \sim 10^{-6}$), despite weak individual carbohydrate−protein binding affinities ($K_d \sim 10^{-3}$) − a well-documented phenomenon termed the "glycoside cluster effect".[22] In this way, nature leverages the power of polymer chemistry to generate selective and specific molecular recognition motifs that are physiologically dynamic.

A fundamental understanding of the macromolecular basis of carbohydrate recognition is essential for deepening our understanding of the natural world,[24−26] as well as to enable the development of new probes and therapeutics. Over the past ∼40 years, a significant body of research has been built up on understanding how carbohydrate multivalency influences function.[24,27−30] Many of these analyses utilize ring opening metathesis polymerization (ROMP) to synthesize glycopolymers for elucidating key structure−function relationships.

Received: September 10, 2024
Revised: October 23, 2024
Accepted: October 24, 2024
Published: November 6, 2024

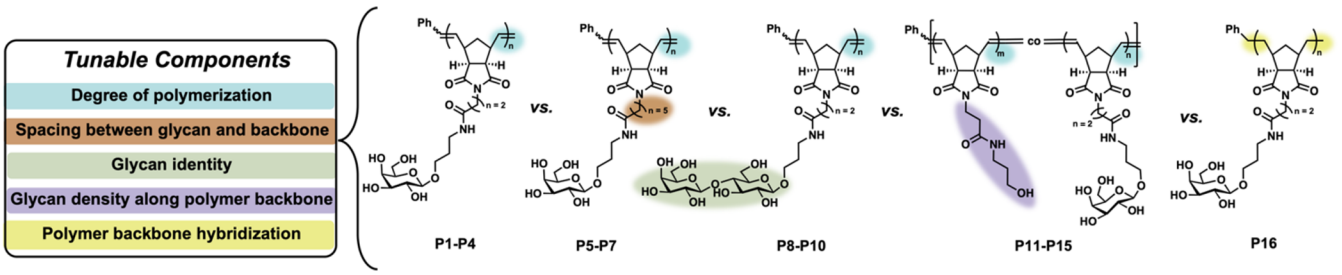

Figure 1. Precision glycopolymer components analyzed herein.

However, the majority of glycopolymers comprise statistical copolymers, utilize graft-to techniques, and/or employ protecting groups that need to be removed post polymerization.[31−36] This results in materials with stochastic local compositions, which restrict batch-to-batch reproducibility and complicate systematic analyses. Indeed, recent developments in discrete glycomacromolecules with absolute sequence control[24] underscore the necessity for well-defined glycomaterials to analyze these complex interactions in a systematic manner.

Motivated by these facts, we sought to understand how the glycan macromolecular conformation dictates glycopolymer properties and lectin recognition. Toward this end, we developed glycopolymer probes with unambiguous local chemical composition and well-defined global macromolecular structure, herein termed precision glycopolymers (PGPs). We reasoned that the graft-through ROMP of unprotected carbohydrates would afford well-defined glycopolymers with maximal grafting density and defined local chemical structure (i.e., each side chain is functionalized, and no postpolymerization manipulations are required). ROMP is ideal in this regard, as it is a controlled polymerization method[37] that allows for the generation of polymers with low dispersity and high reproducibility.[38] Its initiators display excellent functional group tolerance, which permits the incorporation of a diverse array of functionalized monomers, such as the dense concentration of hydroxyl moieties on carbohydrates.[31,39−42] Moreover, the rigid, sp^2-hybridized backbones of poly(norbornene) are akin to the polypeptide backbones on which oligosaccharides are natively displayed.

We used galectin-3 (Gal-3) and peanut agglutinin (PNA) as model systems to analyze the binding of multivalent β-galactosides, representing animal and plant lectins due to their biomedical significance. Gal-3 is involved in myriad physiological processes[43] and in the progression of multiple diseases,[44−46] including cancer. PNA is involved in the recognition and symbiosis of nitrogen-fixing bacteria in peanuts[47,48] and has been shown to promote cancer metastasis by mimicking Gal-3 and differentiating human lymphocytes.[49,50] The natural binding motif of Gal-3 is N-acetyllactosamine (Gal-β(1,4)-GlcNAc),[51] while that of PNA is the Thomsen-Friedenreich antigen (Gal-β(1,3)-GalNAc).[52] As such, the similarity in their binding motifs could offer fundamental insights into the carbohydrate recognition and lectin specificity across species.

Herein, we synthesized PGPs via the direct, graft-through polymerization of galactose and lactose, two β-galactoside ligands (**Gal-PGPs** and **Lac-PGPs**, respectively). We used these materials to evaluate how carbohydrate multivalency and density influence lectin recognition (Figure 1). We found that the multivalent display of carbohydrates drastically overrides differences in individual ligand affinities. Moreover, complete grafting density is required for maximal binding to both Gal-3 and PNA. Coarse-grained (CG) molecular dynamics (MD) simulation analyses provide mechanistic insights into the nature of these interactions, indicating that fully grafted PGPs outperformed others due to decreased carbohydrate-carbohydrate interactions (CCIs), which lead to higher solvent accessible surface area and favorable interactions of carbohydrates with water. This knowledge can be used to guide the design of multivalent lectin-targeting materials for applications in biomaterials and beyond.

EXPERIMENTAL SECTION

General Methods. All materials and reagents, unless otherwise noted, were purchased from either Sigma-Aldrich or Fisher Chemicals. Reagent and their purities are listed as follows: cis-5-Norbornene-exo-2,3-dicarboxylic anhydride (Oakwood, 98%), Triethylamine (Sigma, ≥99.5%), 3-amino-1-propanol (Sigma, 99%), 6-aminohexanoic acid (Alfa Aesar, 99%), β-alanine (Sigma, 99%), *tert*-butyldimethylsilyl chloride (Oakwood, 99%), imidazole (Sigma, ≥99%), 4-dimethylaminopyridine (Acros Organics, 99%), *N*,*N*′-dicyclohexlcarbodiimide (Sigma, 99%), Acetyl chloride (TCI, >98%), β-D-galactose pentaacetate (Sigma, 98%), lactose octaacetate (Sigma, 95%), boron trifluoride diethyl etherate (Sigma, 46−51% BF_3), sodium methoxide (Alfa Aesar, 98%), and ethyl vinyl ether (Sigma, 99%). Dry solvents, dimethylformamide (DMF), dichloromethane (DCM), and methanol (MeOH) were prepared by drying via a VAC solvent purification system (SPS), distillation, and sieves, respectively. Galectin-3 was sourced from Biotechne (Cat# 8259-GA). Peanut agglutinin was sourced from Sigma (Cat# L0881).

Nuclear magnetic resonance spectra were recorded at ambient temperature unless stated otherwise with an Agilent MR 400 (400 MHz), Varian MR-400 (400 MHz), Bruker NEO400 (400 MHz), Bruker AVIII 3 M 500 (500 MHz), or Bruker Avance III HD instrument fitted with a Prodigy cryoprobe (500 MHz). Solvent resonances were referenced for ^{1}H and ^{13}C NMR chemical shifts and reported in ppm. Multiplicity data are reported as s = singlet, d = doublet, t = triplet, q = quartet, p = pentet, and m = multiplet. High resolution ESI-MS was obtained using an Agilent Technologies 6530 Accurate-Mass Q-TOF. Polymer characterization was completed using a Tosoh Bioscience EcoSEC Elite HLC-8420GPC fitted with a TSKgel α-M (0018344) column and a Wyatt DAWN 8 (WD3−03) light scattering detector. The GPC-LS system was run in 10 mM LiBr in DMF at 60 °C. Dynamic light scattering (DLS) measurements were taken by using a Zetasizer Nano ZS.

4T1 cell line was obtained from ATCC. Cells were incubated at 37 °C at 5% CO_2 using RPMI-1640 (Fisher Scientific, Cat: 11875093) supplemented with 10% fetal bovine serum (Fisher Scientific, Cat: 35010CV), and 1% penicillin/streptomycin (Fisher Scientific, Cat: SV30010). Cell cultures were maintained by subculturing in flasks every 2−5 days as necessary per cell growth using trypsin-EDTA, 0.05% (Fisher Scientific, Cat: MT25052Cl).

General Glycopolymer Synthesis. Prior to polymerization, each monomer was dried under high vacuum overnight, then dissolved in freshly dried DMF via a VAC solvent purification system in an oven-dried, N_2-backfilled collection flask. All polymerizations were

https://doi.org/10.1021/acs.biomac.4c01245
Biomacromolecules 2024, 25, 7985−7994

Scheme 1. (a) Structure of Galactose-Based Monomers (Left) and Lactose-Based Monomers (Right); (b) General Ring Opening Metathesis Polymerization Scheme of Glycomonomers to Afford PGPs in a Single Step; and (c) ^{1}H-NMR Analysis of the Polymerization of Mono-Gal$_7$[a]

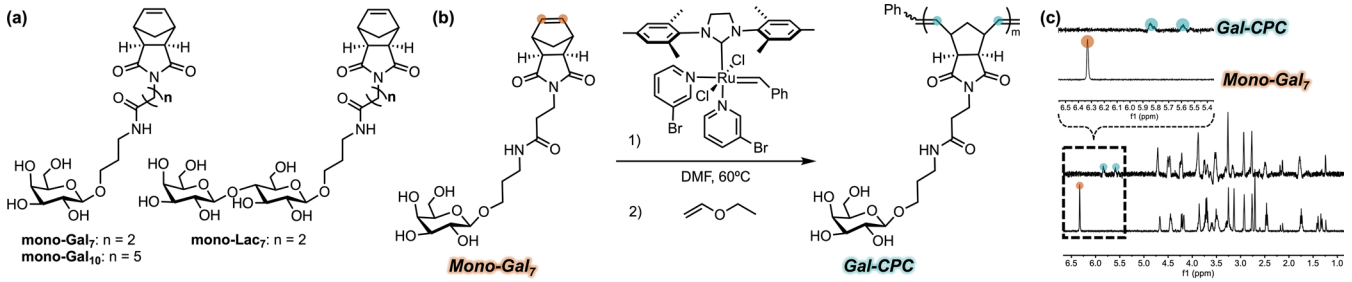

[a]Disappearance of the monomer alkene peak (orange) and appearance of two nonequivalent polymer alkene peaks (blue) indicate complete conversion.

completed in a nitrogen atmosphere in a PLAS-LABORATORIES 810-series glovebox. The monomer (or both monomers for Co-PGP generation) was dissolved in DMF in a microcentrifuge tube at the target monomer-to-catalyst ratio and the polymerization was initiated using the Grubbs M300 catalyst (Sigma: 682330) solution (in DMF) such that the final catalyst concentration was 1.5 mM. The centrifuge tube was then removed from the glovebox and sealed using PTFE tape and parafilm. The reaction was heated at 60 °C while shaking at ∼1200 rpm using a Benchmark Scientific Heating and Cooling Shaker (H5000-HC) for 2−4 h depending on the target polymer length. Polymer termination was accomplished via the addition of ethyl vinyl ether. Polymers were then precipitated from solution using cold diethyl ether and dried under a vacuum. All polymers were then analyzed using SEC-MALS (see SI). See SI for the full experimental details and analysis of P1−P16.

Polymerization Kinetics by ^{1}H NMR. Polymerization kinetics were analyzed at 60 °C in DMF-d$_7$ using a variable temperature NMR. The dissolved monomer was added to an NMR tube fitted with a J. Young valve in a glovebox. The tube was then removed from the box, and an NMR spectrum (t = 0) was obtained in an NMR instrument preheated to 60 °C. The tube was then returned to the glovebox, and the catalyst in DMF-d$_7$ was added to the tube. ^{1}H NMR spectra were then recorded every 120 or 180 s until complete conversion was observed.

Dynamic Light Scattering (DLS) Analysis. Each polymer was dissolved in 18.2 MΩ water (milli-Q water) and placed on a rocker for at least 8 h. The sample was then transferred to a disposable plastic cuvette and was analyzed using a Zetasizer Nano ZS (Dispersant: H_2O RI = 1.330, Viscosity = 0.8872; Material: RI = 1.45, Absorption = 0.001; T = 25 °C) with three runs per measurement, 10 s per run, and at least 3 measurements averaged together.

Surface Plasmon Resonance (SPR) Analysis. Surface Plasmon Resonance (SPR) was used for interaction analysis for all of the lectins. The extent of interaction between the glycopolymers and lectins was analyzed on a BIAcore T200 system (Cytiva Life Sciences). The lectins (0.005 mg/mL) were immobilized *via* a standard amino coupling protocol onto a CM5 sensor chip that was activated by flowing a 1:1 mixture of 0.1 M *N*-hydroxysuccinimide and 0.05 M *N*-ethyl-*N*′ (dimethylaminopropyl)carbodiimide over the chip for 5 min at 25 °C at a flow rate of 5 μL/min after the system equilibration with PBS filtered buffer (10 mM sodium phosphate dibasic heptahydrate and 2 mM sodium phosphate monobasic monohydrate, pH 7.4). Subsequently, channels 1 (blank), 2, 3, and 4 were blocked by flowing a solution of ethanolamine (1 M pH 8.5) for 10 min at 5 μL/min to block the remaining reactive groups on the channels. Sample solutions were prepared at varying concentrations (64−4 μM based on the polymer) in the same PBS buffer to calculate the binding kinetics. Sensorgrams for each glycopolymer concentration were recorded with a 300 s injection of polymer solution (on period), followed by 200 s of buffer alone (off period). Regeneration of the sensor chip surface for PNA was performed using 50 mM NaOH solution and for Galectin-3 using 100 mM NaOH with 0.01% Tween 20 surfactant. A buffer sample was included between each polymer sample during the run. Kinetic data were evaluated using a single set of sites (1:1 Langmuir binding) model in BIAevaluation 3.1 software.

Galectin-3 Western Blot Analysis. Cells (4T1) were washed with PBS and lysed using RIPA buffer with Halt phosphatase and protease inhibitor cocktail (Thermo Fisher: 78440). The protein concentration of the cell lysate was determined using the Pierce BCA assay (Thermo Fisher: 23225, 30 min, 37 °C protocol). Fifteen μg of protein was incubated at 60 °C for 15 min with Laemmli loading dye and 100 mM DTT. Samples were separated in 4−20% SDS-PAGE gel and transferred to a low-fluorescence PVDF membrane. The membrane was blocked with Licor Intercept blocking buffer and then washed with PBST. The membrane was incubated with a 1:500 dilution of antigalectin-3 (Thermo Fisher: 14-5301-82) and 1:2000 dilution of antibeta tubulin (Thermo Fisher: MA516308) in Licor Intercept blocking buffer at 4 °C overnight. Following incubation, the membrane was washed with PBST and then was incubated with 1:1000 dilution of goat antirat 647 (Thermo Fisher: A21247) and 1:1,000 of goat-anti mouse 488 (Thermo Fisher: A28175) in Licor Intercept blocking buffer for 120 min at room temperature in the dark. The membrane was washed with PBST followed by PBS and then imaged with a ChemiDoc Imaging Station.

Cell Viability. Cells were seeded in a 96-well plate at 2500 cells per well. Following growth overnight, cells were treated with PBS, galactose (1 mM), or experimental treatment polymers at final concentrations of 10 μM. At 24 h, the CCK-8 assay (Fisher Scientific: NC9864731) was performed per the manufacturer's instructions. The plate was analyzed by using a BioTek Synergy H1 microplate reader.

Scratch Assay. Cells were seeded in a 24-well plate and allowed to grow until confluent. Following confluence, a p200 micropipet tip was used to make scratches in each well. The media was changed to remove upended cells, and the wells were imaged using a Nikon SMZ800N Stereoscope fitted with a Nikon DS-Ri2 color camera. Wells were then treated with PBS, galactose (1 mM) or experimental treatment polymers at final concentrations of 1, 2.5, 5, or 10 μM. Following treatment for 24 h, cells were imaged, then fixed in 4% PFA and stained with crystal violet. Cells were then imaged again. Analysis of the scratches was completed using ImageJ. The width of each scratch was determined by drawing 10 individual horizontal lines across the scratch, making sure to measure the width along the entirety of the scratched area. All measurements were then averaged together and compared to the average of 10 individual horizontal lines across each scratch over 24 h.

RESULTS AND DISCUSSION

Glycomonomer Design. To probe the effect of multivalency on the binding of galactosides to Gal-3 and PNA, we chose β-galactose and lactose as model ligands, as they are simple naturally occurring glycans recognized by Gal-3[53] and

https://doi.org/10.1021/acs.biomac.4c01245
Biomacromolecules 2024, 25, 7985−7994

Table 1. SEC-MALS Data for the Polymers Used in SPR

entry	class	glycan	linker length	target DP	M_n, theo. (kDa)	M_n, GPC (kDa)	M_w, GPC (kDa)	DP[a]	$Đ$
P1	Homo-Gal$_7$	galactose	7	10	4.5	7.85	8.44	17	1.08
P2	Homo-Gal$_7$	galactose	7	50	22.7	25.9	26.7	57	1.03
P3	Homo-Gal$_7$	galactose	7	100	45.4	48.7	51.7	107	1.06
P4	Homo-Gal$_7$	galactose	7	250	113.6	101.5	128.7	223	1.27
P5	Homo-Gal$_{10}$	galactose	10	10	4.97	4.50	5.06	9	1.14
P6	Homo-Gal$_{10}$	galactose	10	50	24.8	16.5	17.9	33	1.08
P7	Homo-Gal$_{10}$	galactose	10	100	49.7	49.0	52.6	99	1.07
P8	Homo-Lac$_7$	lactose	7	10	6.17	7.65	8.44	12	1.07
P9	Homo-Lac$_7$	lactose	7	50	30.8	29.2	30.9	47	1.06
P10	Homo-Lac$_7$	lactose	7	100	61.7	60.2	66.0	98	1.10
P11	Copoly-Gal:OH	Gal (90), OH (10)	7, 7	100	--	37.1	59.0	--	1.59
P12	Copoly-Gal:OH	Gal (70), OH (30)	7, 7	100	--	48.8	71.5	--	1.45
P13	Copoly-Gal:OH	Gal (50), OH (50)	7, 7	100	--	68.9	102.7	--	1.49
P14	Copoly-Gal:OH	Gal (30), OH (70)	7, 7	100	--	82.6	122.0	--	1.48
P15	Copoly-Gal:OH	Gal (10), OH (90)	7, 7	100	--	67.3	98.8	--	1.47
P16	Gal$_7$ sp^3	galactose	7					107	

[a]DP calculated as $M_n/MW_{monomer}$.

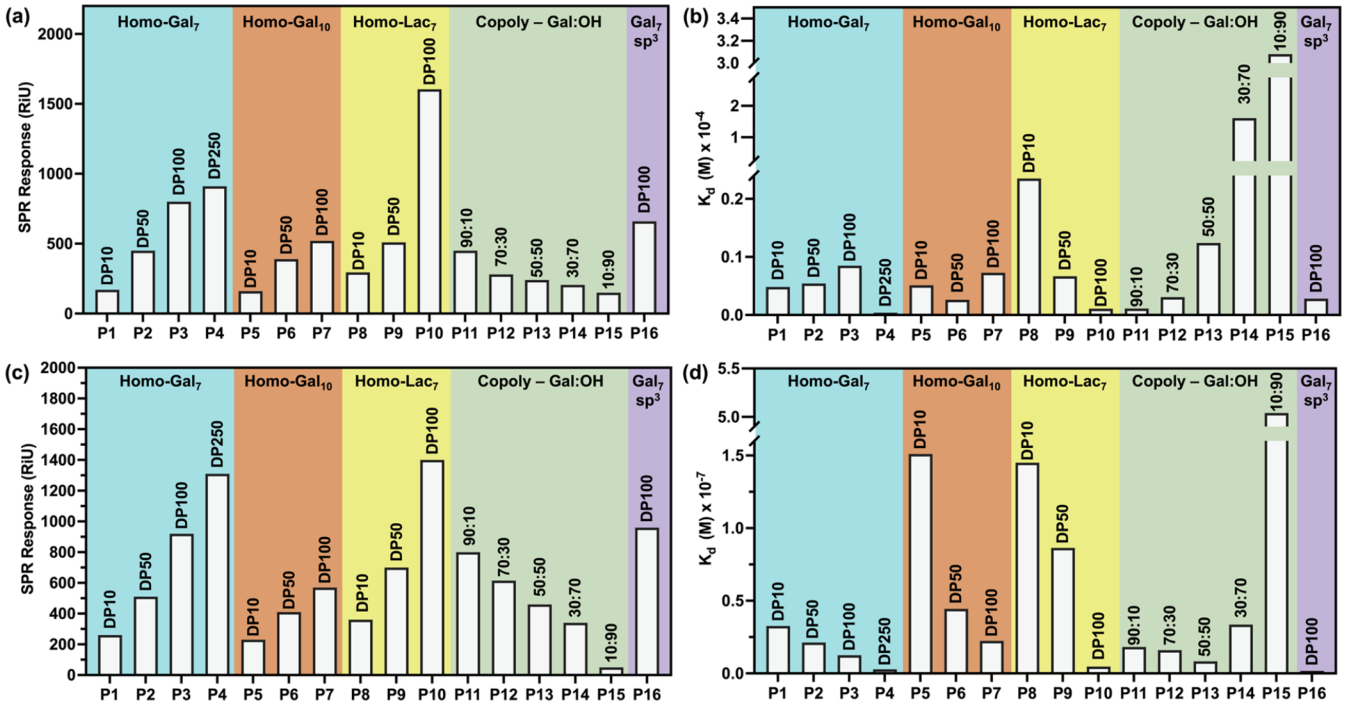

Figure 2. Data visualization for SPR analyses of PNA and Gal-3 binding to polymers P1−P16. (a) Analysis of SPR response units for binding to PNA. (b) Analysis of dissociation constants (K_d) of polymer binding to PNA. (c) Analysis of SPR response units for binding to Gal-3. (d) Analysis of dissociation constants (K_d) of polymer binding to Gal-3.

PNA.[52] β-galactose and lactose have vastly different affinities for Gal-3 (10 mM for galactose, 200 μM for lactose, using isothermal titration calorimetry)[54] and PNA (1 mM for methyl-β-D-Gal, and 769 μM for lactose, using ultraviolet difference spectroscopy).[55] Moreover, previous reports have found that longer linkers on polymer side chains increase self-aggregation from intramolecular hydrophobic and hydrogen bonding.[56] Therefore, we hypothesized that β-galactosides bound by a shorter linker would exhibit improved binding potency compared to those with longer linkers. Thus, we derivatized both galactose and lactose with norbornenyl handles with variations in the spacing between the carbohydrate ligand and polymerizable moiety.

With these design considerations in mind, we synthesized two glycomonomers from galactose (**mono-Gal$_7$** and **mono-Gal$_{10}$**) and one glycomonomer from lactose (**mono-Lac$_7$**) with 7 or 10 atoms between glycan epitope and norbornenyl handle, (Scheme 1a). Briefly, we reacted *cis*-5-Norbornene-*exo*-2,3-dicarboxylic anhydride with an amino acid to afford a norbornenyl dicarboximide, followed by the addition of an amino alcohol using standard amidation conditions. We formed the linker using two components so that we could incorporate an amide, as we hypothesized that a purely hydrocarbon-based linker may overwhelm the hydrophilicity of the carbohydrate and reduce solubility. Moreover, an amide linker provides hydrogen-bonding capability and a way to rapidly change the linker length. Lastly, we conjugated the

https://doi.org/10.1021/acs.biomac.4c01245
Biomacromolecules 2024, 25, 7985−7994

norbornenyl-linker conjugate with a commercially available acetylated sugar to generate a protected glycomonomer that, following deprotection, yields the final glycomonomer with a native glycosidic bond, which we hypothesized may play a role in the recognition of the carbohydrate by Gal-3 and PNA.

Precision Glycopolymer (PGP) Synthesis and Analysis. We subjected each glycomonomer to ROMP using Grubb's third-generation catalyst in dry DMF at 60 °C to afford PGPs (Scheme 1b). Altogether, we synthesized a suite of 16 PGPs from galactose and lactose with variations in linker length (7 or 10 atoms), target degree of polymerization (10, 50, 100, or 250), carbohydrate density (100−10%), and backbone hybridization (sp^2 and sp^3). We attempted to monitor the polymerization progress of mono-Gal_7 by ^1H NMR, but complete conversion occurred in less than 5 min (Scheme 1c). Likewise, all other glycomonomers were also efficiently converted to PGPs within the same time frame (Figures S1−S3). Following polymerization, we characterized all PGPs using size exclusion chromatography with multiangle light scattering (SEC-MALS) to determine the degree of polymerization (DP) and dispersity ($Đ$) (Tables 1 and S1−S4).

Effect of Polymer Scaffold on Lectin Binding. Next, we investigated the binding of all PGPs by Gal-3 and PNA using surface plasmon resonance (SPR). From these analyses, we evaluated the binding interaction between the PGPs and lectins (Figures 2, S4−S7, and Tables S5−S7). Gal-3 and PNA were both conjugated to the chip via standard NHS coupling (RU 13,120 and 9030, respectively, Figures S6 and S7). Following conjugation, the chip was blocked with ethanolamine, and analysis proceeded with the PGPs. We separated the analyses of the PGPs based on polymer scaffold characteristics (polymer length, linker hydrophobicity, and backbone hybridization).

Through these analyses, we found that both the maximum SPR response (R_{max}) and dissociation constant (K_d) between PGPs and Gal-3 increases as a function of polymer length (**P1**−**P4**, **P5**−**P7**, and **P8**−**P10**) for both Gal-PGPs and Lac-PGPs (Figures 2, S5, and Table S6). This indicates that increasing the degree of polymerization generally increases the binding affinity between glycopolymer and lectin due to the multivalent effect, matching previous literature reports.[57,58] This is primarily the result of a faster association rate (k_a) with an initial rapid binding event as the polymers increase in length, which may be due to the increased number of carbohydrates presented to Gal-3 on longer polymers.

All polymers exhibited significantly higher binding affinity to Gal-3 compared to PNA, with approximately 10^3-fold greater values. Notably, all polymers, except for those based on lactose, displayed a saturated binding profile during the association phase, indicating that some lectin binding sites remained unoccupied on the chip. This could be attributed to the limited accessibility and flexibility of the lactose carbohydrates on the polymer chain due to their bulky nature in solution.

When the interactions between PGPs and PNA are evaluated, the same trends in R_{max} and K_d hold for Lac-PGPs (**P8**−**P10**). When analyzing Gal-PGPs (**P1**−**P7**), we find that R_{max} increases with polymer length as expected, but the K_d differences remain within the same order of magnitude until reaching significantly longer lengths (**P4**). This can be explained by comparing the dissociation rate (k_d) to the association rate (k_a) for each polymer (Table S5): the statistical rebinding of ligands (k_a) does not override the polymer release (k_d) until longer polymer lengths are achieved.

When comparing the effect of linker hydrophobicity on PGP binding to both Gal-3 and PNA, R_{max} is decreased for polymers with more hydrophobic linkers (comparing **P1**:**P5**, **P2**:**P6**, and **P3**:**P7**), indicating decreased polymer association with lectins as the hydrophobicity increases. Additionally, as the linker length increases, the entropic penalty for binding also increases, which could be contributing to the lower R_{max} values. However, this does not significantly impact the calculated K_d values for either lectin.

Finally, we compared the effects of polymer backbone hybridization on lectin recognition. A substantial set of literature exists for glycopolymers based on acrylate and acrylamide polymers, which possess sp^3-hybridized backbones.[59−62] As such, we were interested in this study to determine whether the hybridization and rigidity imparted by the alkenes in ROMP based polymers played a critical role in their ability to bind to PNA and Gal-3. To accomplish this, we hydrogenated the backbone of a fully grafted Gal-PGP (**P3**) following literature protocols[63] (see SI Section S4) to afford a fully sp^3-hybridized polymer (**P16**) and evaluated its interaction with both lectins. The calculated K_d was lower for the hydrogenated polymer compared to its alkenyl counterpart for both Gal-3 and PNA, with minimal impact on R_{max}. This difference arises from a significantly slower dissociation rate (k_d) in **P16** compared to **P3**, suggesting that more flexible, sp^3-hybridized polymers associate with lectins for longer. Further investigation revealed that the hydrodynamic radius of **P16** was substantially larger than that of **P3** (43.36 vs 9.53 nm, Table S8 and Figure S8). This indicates that the hydrogenated polymer tends to form multichain aggregates in solution, complicating direct comparisons. However, this aggregation may also account for the rapid association and slow dissociation kinetics observed, as the multichain aggregates present a higher density of binding moieties compared with a fully solvated polymer. Overall, the polymers demonstrated low dissociation rate constants (k_d, s^{-1}), indicating that strong interactions with the galactose units on the side chains are persistent or that rebinding of released galactose units occurs more quickly than the dissociation of the complex during the buffer wash period.

Effect of Glycan Epitope Density and Identity on Lectin Binding. In addition to probing the effect of polymer scaffold on lectin binding, we also investigated how changing characteristics of the glycan epitope (identity and density) impact recognition. These variables were selected based on prior findings highlighting the importance of both density and valency in lectin binding.[64] Toward this end, we synthesized a "diluent" monomer, which contained a single hydroxyl moiety (**mono**−**OH**) in place of the glycan epitope (see Scheme S1). We then synthesized copolymers together with mono-Gal_7 using ROMP at a target degree of polymerization of 100 and a feed ratio of 9:1, 7:3, 1:1, 3:7, and 1:9 feed ratios of galactose:diluent, respectively, to mimic polymers at 90, 70, 50, 30 and 10% overall grafting density (**P11**−**P15**, Table 1). We note that these polymers, possessing greater inherent dispersity, are not considered "PGPs" and instead are referred to as copolymers throughout the text.

In all cases, decreasing the density of the polymers has minimal impact on the binding affinity for both Gal-3 and PNA until the overall glycan density drops below 50% (**P3** vs **P11**−**P15**, Figure 2). However, the R_{max} decreases steadily as

https://doi.org/10.1021/acs.biomac.4c01245
Biomacromolecules 2024, 25, 7985−7994

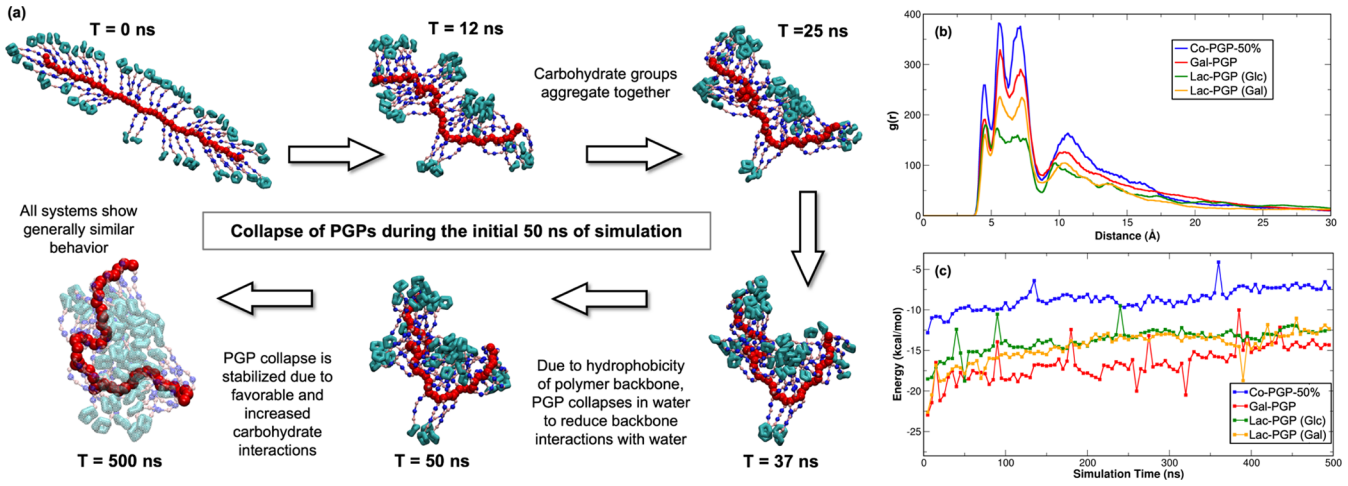

Figure 3. Coarse-grained molecular dynamics analyses. (a) Representative schematic for the collapse of PGPs during the initial 50 ns of the simulation trajectory and a conformation at the end of 500 ns of CG MD simulations. The hydrophobic norbornene backbone is colored red, whereas the carbohydrate functional groups are colored cyan. (b) Radial distribution function (RDF) between centers-of-mass (COMs) of attached monosaccharide groups on the PGPs, calculated for the last 150 ns of the simulation run. (c) Evolution of the nonbonded interaction energy between monosaccharide groups and water throughout the simulation run.

polymer density decreases for both lectins, indicating that increasing the grafting density increases the overall association with lectins. This is reflected in decreased association rates (k_a) for polymers with decreased glycan densities for both lectins. Taken together, these data indicate that 50% glycan density is a critical point for lectin binding affinity. Additionally, the increased association rates of fully grafted polymers suggest that higher grafting densities may be advantageous for applications where glycopolymers are in complex, dynamic environments (e.g., the extracellular matrix). When comparing polymers with similar sugar content but differing densities and lengths (**P1** vs **P15**, **P2** vs **P13**, and **P3** vs **P11**, Figure 2) a similar trend is also observed. For Gal-3, the R_{max} decreases and the K_d increases once the polymer density drops below 50%. This trend continues for PNA but extends above 50% density, where a density reduction at all leads to a lower R_{max} and higher K_d.

Regarding glycan epitope identity, R_{max} is higher in Lac-PGPs as compared to Gal-PGPs at each degree of polymerization (**P1** vs **P8**, **P2** vs **P9**, **P3** vs **P10**) for both Gal-3 and PNA. This suggests that Lac-PGPs interact more with these lectins than their galactose-based counterparts. In addition, the overall degree of polymerization has a greater impact on lactose-based PGPs than on galactose-based PGPs for both Gal-3 and PNA. For both lectins, a sharp decrease in K_d is observed when increasing the degree of polymerization of lactose-based PGPs from 10 to 50 (**P8**−**P9**) and from 50 to 100 (**P9**−**P10**). Conversely, these differences are attenuated for galactose-based PGPs (**P1**−**P4**) until high degrees of polymerization (ca. 250) are achieved. Lastly, a clear trend is observed when considering the overall binding of PGPs to Gal-3 compared to PNA, where PGPs bind better to Gal-3 than PNA in every instance. This is largely the result of slower disassociation rates (k_d) of PGPs from Gal-3, indicating that much tighter and longer-lasting interactions are occurring with this lectin-glycopolymer pair.

Based on the data, it is evident that protein-glycopolymer interactions are highly complex and are influenced by a multitude of variables. For these systems, the epitope density and polymer length are the most critical for strong binding to both PNA and Gal-3. Both of these parameters will change the overall rigidity and hydrophobicity of the polymer structure and thus likely influence solution morphology. As such, we sought to investigate the solution behavior of these materials by using computational models to more fully elucidate the basis for these differences.

Coarse-Grained Molecular Dynamics Simulations. To investigate PGP conformations in solution, we employed coarse-grained (CG) molecular dynamics (MD) simulations, which enable studying large molecular systems like bottlebrush polymers (BBPs) for several microseconds.[65,66] To probe the effect of grafting density on PGP conformation, we simulated three types of PGPs with grafting densities similar to those used in our experiments. Here, we utilized transferable CG models of peptides,[67,68] hydrocarbons,[69,70] and carbohydrates to model and simulate PGPs in explicit water. CG MD simulations were carried out for three initial configurations for each system, on the Nanoscale Molecular Dynamics (NAMD) simulation package using the NPT (T = 298 K) ensemble for 500 ns.[71] More details regarding the mapping schemes, CG models, and simulation details can be found in the SI (Figures S9−S20 and Tables S9−S11).

Visual inspection of CG MD simulation trajectories revealed that all PGPs collapsed into globular aggregates within the initial 100 ns (Figure 3a) and that this aggregation was driven by carbohydrate-carbohydrate interactions. In all cases, the first aggregation event is between monosaccharide functional groups. This was then followed by the collapse of the hydrophobic PGP backbones to reduce backbone interactions with water. This collapse of the PGP backbone was simultaneously stabilized through the increased carbohydrate aggregation, which resulted in equilibrated globular structures with aspect ratios of 0.68 ± 0.12, 0.71 ± 0.10, and 0.69 ± 0.10 for Lac-PGP, Gal-PGP, and Co-PGP-50% systems, respectively. Additionally, following equilibration, radius of gyration (R_g) values for Lac-PGP systems fluctuated around a mean value of 2.18 ± 0.4 nm compared to 1.77 ± 0.1 and 1.77 ± 0.2 nm of Gal-PGP and Co-PGP-50% systems, which were much lower than the R_g values of stretched PGPs (Figure S17). Based on aspect ratios and R_g values for these globule-like

https://doi.org/10.1021/acs.biomac.4c01245
Biomacromolecules 2024, 25, 7985−7994

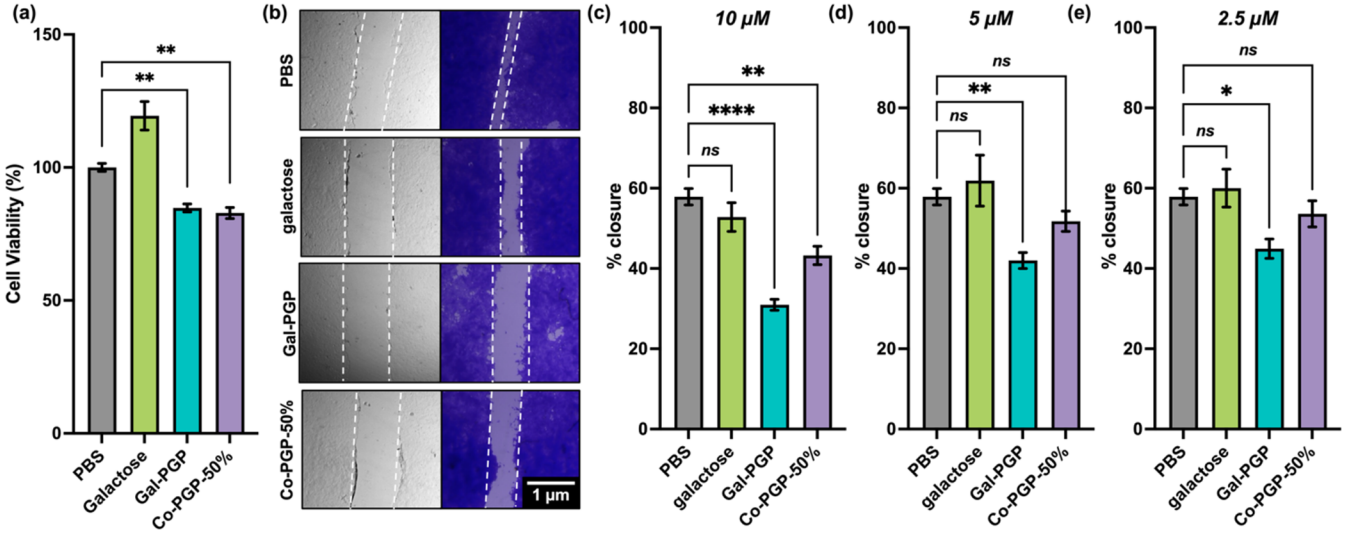

Figure 4. (a) Effect of treatment on cancer cell viability following 24 h incubation. Gal-PGPs effectively effectively suppress cancer cell proliferation in Gal-3-positive 4T1 cells. (b) Antimigration activities of Gal-PGPs. Cells were stained with crystal violet to enhance contrast and facilitate analysis. Representative images of scratched 4T1 cells before treatment (left) and after 24 h incubation with various constructs (right). All polymers show dose-dependent inhibition of 4T1 cell migration. (c) Comparison of antimigration efficacy of polymers at 10 μM. At this dose, all constructs are able to suppress the migration of 4T1 cells; however, Gal-PGPs significantly outperform all other treatment groups. (d) Comparison of antimigration efficacy of PGPs at 5 μM. (e) Comparison of antimigration efficacy of PGPs at 2.5 μM. Statistical analysis was performed using an ordinary one-way ANOVA, where "*" represents a P value of <0.05, "**" represents a P value of <0.01, "***" represents a P value of <0.001, and "****" represents a P value of <0.0001.

structures, we utilized the relation $R_g/R_h \approx 0.78$ to estimate the hydrodynamic radii (R_h) of our PGPs.[72,73] These values for the Lac-PGP, Gal-PGP, and Co-PGP-50% systems were 2.79, 2.27, and 2.27 nm, respectively. These data were in good agreement with our experimental R_h values, measured via dynamic light scattering (DLS, Table S8), for Lac-PGPs (R_h = 3.4 nm), Gal-PGPs (R_h = 2.6 nm), and the statistical copolymer (R_h = 2.5 nm).

To examine microscopic structural correlations in the system, we calculated the radial distribution functions (RDFs) between different bead types (Figure S18). RDFs between the PGP backbone and water showed greater hydration of the Lac-PGP system, followed by the Gal-PGP and Co-PGP-50% systems. Similarly, RDFs between monosaccharide groups in the PGPs with water showed similar structural correlations, with slightly greater hydration for the monosaccharide groups in the Lac-PGP system. RDFs between monosaccharide groups that are known to be important for binding to Gal-3 showed that the structural correlation between monosaccharide groups was highest for Co-PGP-50% systems compared to homopolymers Lac-PGP and Gal-PGP (Figure 3b). These data indicate that the homopolymer systems show more exposure of monosaccharide groups to the solvent, whereas for the Co-PGP-50% system, monosaccharide groups are more strongly aggregated, indicating increased CCIs in the copolymer system.

Given the role of water in carbohydrate-lectin recognition,[74] we evaluated the interaction of each system with water. Structural correlations between water and monosaccharide groups follow the order: Lac-PGP > Gal-PGP > Co-PGP-50%. Similarly, the solvent accessible surface area (SASA) values for all systems were calculated, showing the highest values for the Lac-PGP system followed by Gal-PGP and Co-PGP-50% systems (Figure S19). This arises from stronger aggregation between monosaccharide groups in Co-PGP-50% as compared to the rest, thus further validating the RDF data. Additionally, the nonbonded energies between different groups in the systems were isolated and obtained for the entire trajectory (Figure S20). While the nonbonded energies between backbone-water and between monosaccharide groups showed similar values in all PGP systems, a clear difference was observed for energies between monosaccharide groups and water (Figure 3c). The interaction energy with water was found to be the lowest with monosaccharide groups in the Gal-PGP system, indicating the most favorable interactions. This was followed by the monosaccharide groups in the Lac-PGP system, whereas the Co-PGP-50% system exhibited the most unfavorable interactions with water. These data complement our prior observations, indicating that monosaccharide groups in Gal-PGP and Lac-PGP systems show more favorable interactions with water, thus making them available for binding to Gal-3 and PNA.

Biological Activity of Gal-PGPs. To evaluate whether differences in protein binding and solution behavior translate to meaningful differences in biological activity, we assessed the effect of a fully grafted Gal-PGP (DP = 100, **P23**, Table S3) on cellular viability and cellular migration in 4T1 triple negative breast cancer (TNBC) cells, as compared to a galactose-based copolymer at 50% density (Co-PGP-50%, **P24**, Table S3). 4T1 cells express a multitude of galectins,[75−77] including Gal-3 (Figure S21) and mimic human Stage IV breast cancer. After 24 h of incubation, both Gal-PGP and Co-PGP-50% significantly reduced cellular viability as compared to saline (Figure 4a). Conversely, the monosaccharide galactose did not inhibit cell viability at the same overall galactose concentration and in fact appears to promote cell growth, potentially as a result of galactose metabolism.[78] In addition, both Gal-PGP and Co-PGP-50% significantly impeded cell migration at 24 h (Figure 4b,c), while monosaccharide galactose had no effect. Together, this indicates that multivalent presentation can be used to turn innocuous sugars into functional materials that inhibit cancer growth. In evaluating the effect of grafting

https://doi.org/10.1021/acs.biomac.4c01245
Biomacromolecules 2024, 25, 7985−7994

density on biological performance, Gal-PGPs were able to significantly suppress cell migration at all concentrations tested (Figure 4), whereas Co-PGP-50% was effective only at high concentrations. This suggests that full grafting density is required for maximum biological response.

CONCLUSIONS

The complex, multifunctional role of carbohydrates in biology relies, not solely on their molecular composition, but also on their broader macro- and supramolecular architecture. Motivated by this, we designed PGPs as a tool to systematically investigate how variations in polymer architecture influence the binding interactions of glycopolymers with PNA and Gal-3. Our investigations have found that while all polymer parameters play a role in forming high avidity interactions, polymer length and epitope density are critical factors for developing effective glycopolymers against PNA and Gal-3. This finding is consistent with other reports on multivalent glycan-lectin interactions, which shows that increased sugar density enhances the binding affinity between lectins and glycopolymers[79] or dendrimers.[80] Notably, both our work and previous reports differ from observations in nanoscale multivalent architectures,[81] where higher sugar density reduces protein binding. This discrepancy may be due to the distinct 3D conformations on the nanoscale, emphasizing the need for further investigation. When analyzing these interactions on a per-glycan basis, we observe trends consistent with the literature, where the contribution of each glycan to both R_{max} and the K_d is reduced as polymer length increases (Table S7). Coarse-grained molecular dynamics simulations reveal that reduced CCIs in the fully grafted PGPs increase the solvent accessible surface area and carbohydrate-water interactions become more favorable, offering valuable insights into the hierarchical organization of glycans and their mode of interaction with PNA and Gal-3. Thus, these materials not only advance our fundamental understanding of macromolecular glycans in biology but also offer a potential pathway to the development of new functional biomaterials from readily available simple β-galactosides.

ASSOCIATED CONTENT

Supporting Information

The Supporting Information is available free of charge at https://pubs.acs.org/doi/10.1021/acs.biomac.4c01245.

Specific synthesis procedures, NMR data, polymer synthesis and characterization, SPR traces and values, DLS analysis, coarse-grained molecular dynamics simulations, and Gal-3 Western blot (PDF)

AUTHOR INFORMATION

Corresponding Author

Cassandra E. Callmann − *Department of Chemistry, The University of Texas at Austin, Austin, Texas 78712, United States;* orcid.org/0000-0003-1561-3240; Email: ccallmann@utexas.edu

Authors

Cole A. Williams − *Department of Chemistry, The University of Texas at Austin, Austin, Texas 78712, United States*

Daniel J. Stone − *Department of Chemistry, The University of Texas at Austin, Austin, Texas 78712, United States*

Soumil Y. Joshi − *Department of Chemical Engineering, Virginia Tech, Blacksburg, Virginia 24061, United States;* orcid.org/0000-0003-1531-0098

Gokhan Yilmaz − *Department of Chemistry, University of Warwick, Coventry CV4 7AL, U.K.*

Parisa Farzeen − *Department of Chemical Engineering, Virginia Tech, Blacksburg, Virginia 24061, United States*

Sungjin Jeon − *Department of Chemistry, The University of Texas at Austin, Austin, Texas 78712, United States;* orcid.org/0009-0002-2450-6527

Zamira Harris-Ryden − *Department of Chemistry, The University of Texas at Austin, Austin, Texas 78712, United States*

C. Remzi Becer − *Department of Chemistry, University of Warwick, Coventry CV4 7AL, U.K.;* orcid.org/0000-0003-0968-6662

Sanket A. Deshmukh − *Department of Chemical Engineering, Virginia Tech, Blacksburg, Virginia 24061, United States;* orcid.org/0000-0001-7573-0057

Complete contact information is available at: https://pubs.acs.org/10.1021/acs.biomac.4c01245

Author Contributions

‖C.A.W. and D.J.S. contributed equally to this work.

Notes

The authors declare no competing financial interest.

ACKNOWLEDGMENTS

The authors acknowledge funding and support from GlycoMIP, a National Science Foundation Materials Innovation Platform (DMR-1933525). C.E.C. acknowledges funding support from the Cancer Prevention and Research Institute of Texas (RR210050), the Welch Foundation (F-2093-20220331), and the American Cancer Society (IRG-21-135-01-IRG). S.A.D., S.Y.J., and P.F. acknowledge the Advanced Research Computing Facility at Virginia Tech. The authors also thank NIH grant 1 S10 OD021508-1 for use of the Bruker AVANCE III 500 NMR at UT-Austin.

REFERENCES

(1) Godula, K.; Bertozzi, C. R. Density Variant Glycan Microarray for Evaluating Cross-Linking of Mucin-like Glycoconjugates by Lectins. *J. Am. Chem. Soc.* **2012**, *134* (38), 15732−15742.

(2) Cobb, B. A.; Kasper, D. L. Coming of age: carbohydrates and immunity. *Eur. J. Immunol.* **2005**, *35* (2), 352−356.

(3) Hendrikse, S. I. S.; Su, L.; Hogervorst, T. P.; Lafleur, R. P. M.; Lou, X.; van der Marel, G. A.; Codee, J. D. C.; Meijer, E. W. Elucidating the Ordering in Self-Assembled Glycocalyx Mimicking Supramolecular Copolymers in Water. *J. Am. Chem. Soc.* **2019**, *141* (35), 13877−13886.

(4) Bertozzi, C. R.; Kiessling, L. L. Chemical Glycobiology. *Science* **2001**, *291* (5512), 2357.

(5) Richards, S.-J.; Gibson, M. I. Toward Glycomaterials with Selectivity as Well as Affinity. *JACS Au* **2021**, *1* (12), 2089−2099.

(6) Lutz, T. M.; Kimna, C.; Casini, A.; Lieleg, O. Bio-based and bio-inspired adhesives from animals and plants for biomedical applications. *Mater. Today Bio* **2022**, *13*, No. 100203.

(7) Singh, A.; Arango, J. C.; Shi, A.; d'Aliberti, J. B.; Claridge, S. A. Surface-Templated Glycopolymer Nanopatterns Transferred to Hydrogels for Designed Multivalent Carbohydrate−Lectin Interactions across Length Scales. *J. Am. Chem. Soc.* **2023**, *145* (3), 1668−1677.

(8) Isono, T.; Nakahira, S.; Hsieh, H.-C.; Katsuhara, S.; Mamiya, H.; Yamamoto, T.; Chen, W.-C.; Borsali, R.; Tajima, K.; Satoh, T.

Carbohydrates as Hard Segments for Sustainable Elastomers: Carbohydrates Direct the Self-Assembly and Mechanical Properties of Fully Bio-Based Block Copolymers. *Macromolecules* **2020**, *53* (13), 5408−5417.
(9) Echeverri, D.; Orozco, J. Glycan-Based Electrochemical Biosensors: Promising Tools for the Detection of Infectious Diseases and Cancer Biomarkers. *Molecules* **2022**, *27* (23), 8533.
(10) Mancini, R. J.; Lee, J.; Maynard, H. D. Trehalose Glycopolymers for Stabilization of Protein Conjugates to Environmental Stressors. *J. Am. Chem. Soc.* **2012**, *134* (20), 8474−8479.
(11) Stenzel, M. H. Glycopolymers for Drug Delivery: Opportunities and Challenges. *Macromolecules* **2022**, *55* (12), 4867−4890.
(12) Clauss, Z. S.; Wardzala, C. L.; Schlirf, A. E.; Wright, N. S.; Saini, S. S.; Onoa, B.; Bustamante, C.; Kramer, J. R. Tunable, biodegradable grafting-from glycopolypeptide bottlebrush polymers. *Nat. Commun.* **2021**, *12* (1), No. 6472.
(13) Gim, S.; Zhu, Y.; Seeberger, P. H.; Delbianco, M. Carbohydrate-based nanomaterials for biomedical applications. *WIREs Nanomed. Nanobiotechnol.* **2019**, *11* (5), No. e1558.
(14) Zhao, T.; Terracciano, R.; Becker, J.; Monaco, A.; Yilmaz, G.; Becer, C. R. Hierarchy of Complex Glycomacromolecules: From Controlled Topologies to Biomedical Applications. *Biomacromolecules* **2022**, *23* (3), 543−575.
(15) Mastrotto, F.; Pirazzini, M.; Negro, S.; Salama, A.; Martinez-Pomares, L.; Mantovani, G. Sulfation at Glycopolymer Side Chains Switches Activity at the Macrophage Mannose Receptor (CD206) In Vitro and In Vivo. *J. Am. Chem. Soc.* **2022**, *144* (50), 23134−23147.
(16) O'Leary, T. R.; Critcher, M.; Stephenson, T. N.; Yang, X.; Hassan, A. A.; Bartfield, N. M.; Hawkins, R.; Huang, M. L. Chemical editing of proteoglycan architecture. *Nat. Chem. Biol.* **2022**, *18* (6), 634−642.
(17) Restuccia, A.; Fettis, M. M.; Hudalla, G. A. Glycomaterials for immunomodulation, immunotherapy, and infection prophylaxis. *J. Mater. Chem. B* **2016**, *4* (9), 1569−1585.
(18) Thodikayil, A. T.; Sharma, S.; Saha, S. Engineering Carbohydrate-Based Particles for Biomedical Applications: Strategies to Construct and Modify. *ACS Appl. Bio Mater.* **2021**, *4* (4), 2907−2940.
(19) Purcell, S. C.; Godula, K. Synthetic glycoscapes: addressing the structural and functional complexity of the glycocalyx. *Interface Focus* **2019**, *9* (2), No. 20180080.
(20) Chen, S.; Qin, R.; Mahal, L. K. Sweet systems: technologies for glycomic analysis and their integration into systems biology. *Crit. Rev. Biochem. Mol. Biol.* **2021**, *56* (3), 301−320.
(21) Dam, T. K.; Brewer, C. F. Lectins as pattern recognition molecules: The effects of epitope density in innate immunity*. *Glycobiology* **2010**, *20* (3), 270−279.
(22) Miura, Y.; Hoshino, Y.; Seto, H. Glycopolymer Nanobiotechnology. *Chem. Rev.* **2016**, *116* (4), 1673−1692.
(23) Ng, L.; Grodzinsky, A. J.; Patwari, P.; Sandy, J.; Plaas, A.; Ortiz, C. Individual cartilage aggrecan macromolecules and their constituent glycosaminoglycans visualized via atomic force microscopy. *J. Struct. Biol.* **2003**, *143* (3), 242−257.
(24) Hartweg, M.; Jiang, Y.; Yilmaz, G.; Jarvis, C. M.; Nguyen, H. V.; Primo, G. A.; Monaco, A.; Beyer, V. P.; Chen, K. K.; Mohapatra, S.; Axelrod, S.; Gómez-Bombarelli, R.; Kiessling, L. L.; Becer, C. R.; Johnson, J. A. Synthetic Glycomacromolecules of Defined Valency, Absolute Configuration, and Topology Distinguish between Human Lectins. *JACS Au* **2021**, *1* (10), 1621−1630.
(25) Kiessling, L. L.; Grim, J. C. Glycopolymer probes of signal transduction. *Chem. Soc. Rev.* **2013**, *42* (10), 4476−4491.
(26) Huang, M. L.; Godula, K. Nanoscale materials for probing the biological functions of the glycocalyx. *Glycobiology* **2016**, *26* (8), 797−803.
(27) Gordon, E. J.; Strong, L. E.; Kiessling, L. L. Glycoprotein-inspired materials promote the proteolytic release of cell surface l-Selectin. *Bioorg. Med. Chem.* **1998**, *6* (8), 1293−1299.
(28) Lees, W. J.; Spaltenstein, A.; Kingery-Wood, J. E.; Whitesides, G. M. Polyacrylamides Bearing Pendant.alpha.-Sialoside Groups Strongly Inhibit Agglutination of Erythrocytes by Influenza A Virus: Multivalency and Steric Stabilization of Particulate Biological Systems. *J. Med. Chem.* **1994**, *37* (20), 3419−3433.
(29) Abdouni, Y.; Yilmaz, G.; Monaco, A.; Aksakal, R.; Becer, C. R. Effect of Arm Number and Length of Star-Shaped Glycopolymers on Binding to Dendritic and Langerhans Cell Lectins. *Biomacromolecules* **2020**, *21* (9), 3756−3764.
(30) Pieters, R. J. Maximising multivalency effects in protein−carbohydrate interactions. *Org. Biomol. Chem.* **2009**, *7* (10), 2013−2025.
(31) Manning, D. D.; Hu, X.; Beck, P.; Kiessling, L. L. Synthesis of Sulfated Neoglycopolymers: Selective P-Selectin Inhibitors. *J. Am. Chem. Soc.* **1997**, *119* (13), 3161−3162.
(32) Strong, L. E.; Kiessling, L. L. A General Synthetic Route to Defined, Biologically Active Multivalent Arrays. *J. Am. Chem. Soc.* **1999**, *121* (26), 6193−6196.
(33) Kamitakahara, H.; Suzuki, T.; Nishigori, N.; Suzuki, Y.; Kanie, O.; Wong, C.-H. A Lysoganglioside/Poly-L-glutamic Acid Conjugate as a Picomolar Inhibitor of Influenza Hemagglutinin. *Angew. Chem., Int. Ed.* **1998**, *37* (11), 1524−1528.
(34) Mammen, M.; Dahmann, G.; Whitesides, G. M. Effective Inhibitors of Hemagglutination by Influenza Virus Synthesized from Polymers Having Active Ester Groups. Insight into Mechanism of Inhibition. *J. Med. Chem.* **1995**, *38* (21), 4179−4190.
(35) Sheng, G. J.; Oh, Y. I.; Chang, S.-K.; Hsieh-Wilson, L. C. Tunable Heparan Sulfate Mimetics for Modulating Chemokine Activity. *J. Am. Chem. Soc.* **2013**, *135* (30), 10898−10901.
(36) Oh, Y. I.; Sheng, G. J.; Chang, S.-K.; Hsieh-Wilson, L. C. Tailored Glycopolymers as Anticoagulant Heparin Mimetics. *Angew. Chem., Int. Ed.* **2013**, *52* (45), 11796−11799.
(37) Bielawski, C. W.; Grubbs, R. H. Living ring-opening metathesis polymerization. *Prog. Polym. Sci.* **2007**, *32* (1), 1−29.
(38) Jeon, S.; Haynie, T.; Chung, S.; Callmann, C. E. Bioinspired, Carbohydrate-Containing Polymers Efficiently and Reversibly Sequester Heavy Metals. *ACS Cent. Sci.* **2024**, *10* (9), 1782−1788.
(39) Mortell, K. H.; Gingras, M.; Kiessling, L. L. Synthesis of cell agglutination inhibitors by aqueous ring-opening metathesis polymerization. *J. Am. Chem. Soc.* **1994**, *116* (26), 12053−12054.
(40) Kanai, M.; Mortell, K. H.; Kiessling, L. L. Varying the Size of Multivalent Ligands: The Dependence of Concanavalin A Binding on Neoglycopolymer Length. *J. Am. Chem. Soc.* **1997**, *119* (41), 9931−9932.
(41) Tang, S.; Puryear, W. B.; Seifried, B. M.; Dong, X.; Runstadler, J. A.; Ribbeck, K.; Olsen, B. D. Antiviral Agents from Multivalent Presentation of Sialyl Oligosaccharides on Brush Polymers. *ACS Macro Lett.* **2016**, *5* (3), 413−418.
(42) Fraser, C.; Grubbs, R. H. Synthesis of Glycopolymers of Controlled Molecular Weight by Ring-Opening Metathesis Polymerization Using Well-Defined Functional Group Tolerant Ruthenium Carbene Catalysts. *Macromolecules* **1995**, *28* (21), 7248−7255.
(43) Joeh, E.; O'Leary, T.; Li, W.; Hawkins, R.; Hung, J. R.; Parker, C. G.; Huang, M. L. Mapping glycan-mediated galectin-3 interactions by live cell proximity labeling. *Proc. Natl. Acad. Sci. U.S.A.* **2020**, *117* (44), 27329−27338.
(44) Califice, S.; Castronovo, V.; Van Den Brûle, F. Galectin-3 and cancer (Review). *Int. J. Oncol.* **2004**, *25* (4), 983−1075.
(45) Feilchenfeldt, J.; Tötsch, M.; Sheu, S.-Y.; Robert, J.; Spiliopoulos, A.; Frilling, A.; Schmid, K. W.; Meier, C. A. Expression of Galectin-3 in Normal and Malignant Thyroid Tissue by Quantitative PCR and Immunohistochemistry. *Mod. Pathol.* **2003**, *16* (11), 1117−1123.
(46) Gao, P.; Simpson, J. L.; Zhang, J.; Gibson, P. G. Galectin-3: its role in asthma and potential as an anti-inflammatory target. *Respir. Res.* **2013**, *14* (1), 136.
(47) Bhagwat, A. A.; Thomas, J. Dual Binding Sites for Peanut Lectin on Rhizobia. *Microbiology* **1980**, *117* (1), 119−125.
(48) Mody, B.; Mody, R.; Modi, V. Peanut agglutinin-induced structural changes in cowpea Rhizobia as revealed by freeze-etching. *Curr. Microbiol.* **1990**, *21* (4), 243−247.

https://doi.org/10.1021/acs.biomac.4c01245
Biomacromolecules 2024, 25, 7985−7994

(49) Wang, W.; Sindrewicz-Goral, P.; Chen, C.; Duckworth, C. A.; Pritchard, D. M.; Rhodes, J. M.; Yu, L. G. Appearance of peanut agglutinin in the blood circulation after peanut ingestion promotes endothelial secretion of metastasis-promoting cytokines. *Carcinogenesis* **2021**, *42* (8), 1079−1088.
(50) Reisner, Y.; Biniaminov, M.; Rosenthal, E.; Sharon, N.; Ramot, B. Interaction of peanut agglutinin with normal human lymphocytes and with leukemic cells. *Proc. Natl. Acad. Sci. U.S.A.* **1979**, *76* (1), 447−451.
(51) Bumba, L.; Laaf, D.; Spiwok, V.; Elling, L.; Křen, V.; Bojarová, P. Poly-N-Acetyllactosamine Neo-Glycoproteins as Nanomolar Ligands of Human Galectin-3: Binding Kinetics and Modeling. *Int. J. Mol. Sci.* **2018**, *19* (2), 372.
(52) Natchiar, S. K.; Suguna, K.; Surolia, A.; Vijayan, M. Peanut agglutinin, a lectin with an unusual quaternary structure and interesting ligand binding properties. *Crystallogr. Rev.* **2007**, *13* (1), 3−28.
(53) Nio-Kobayashi, J.; Itabashi, T. Galectins and Their Ligand Glycoconjugates in the Central Nervous System Under Physiological and Pathological Conditions. *Front. Neuroanat.* **2021**, *15*, No. 767330, DOI: 10.3389/fnana.2021.767330.
(54) Saraboji, K.; Håkansson, M.; Genheden, S.; Diehl, C.; Qvist, J.; Weininger, U.; Nilsson, U. J.; Leffler, H.; Ryde, U.; Akke, M.; Logan, D. T. The Carbohydrate-Binding Site in Galectin-3 Is Preorganized To Recognize a Sugarlike Framework of Oxygens: Ultra-High-Resolution Structures and Water Dynamics. *Biochemistry* **2012**, *51* (1), 296−306.
(55) Neurohr, K. J.; Young, N. M.; Mantsch, H. H. Determination of the carbohydrate-binding properties of peanut agglutinin by ultraviolet difference spectroscopy. *J. Biol. Chem.* **1980**, *255* (19), 9205−9209.
(56) Mosquera-Giraldo, L. I.; Borca, C. H.; Meng, X.; Edgar, K. J.; Slipchenko, L. V.; Taylor, L. S. Mechanistic Design of Chemically Diverse Polymers with Applications in Oral Drug Delivery. *Biomacromolecules* **2016**, *17* (11), 3659−3671.
(57) Zhou, C.; Reesink, H. L.; Putnam, D. A. Selective and Tunable Galectin Binding of Glycopolymers Synthesized by a Generalizable Conjugation Method. *Biomacromolecules* **2019**, *20* (10), 3704−3712.
(58) Gonnot, C.; Scalabrini, M.; Roubinet, B.; Ziane, C.; Boeda, F.; Deniaud, D.; Landemarre, L.; Gouin, S. G.; Fontaine, L.; Montembault, V. ROMP-based Glycopolymers with High Affinity for Mannose-Binding Lectins. *Biomacromolecules* **2023**, *24* (8), 3689−3699.
(59) Matsuoka, K.; Kaneshima, T.; Adachi, R.; Sasaki, J.; Hashiguchi, T.; Koyama, T.; Matsushita, T.; Hatano, K. Preparation of glycopolymers having sialyl $\alpha 2 \rightarrow 3$ lactose moieties as the potent inhibitors for mumps virus. *Bioorg. Med. Chem. Lett.* **2021**, *52*, No. 128389.
(60) Richards, S.-J.; Jones, M. W.; Hunaban, M.; Haddleton, D. M.; Gibson, M. I. Probing Bacterial-Toxin Inhibition with Synthetic Glycopolymers Prepared by Tandem Post-Polymerization Modification: Role of Linker Length and Carbohydrate Density. *Angew. Chem., Int. Ed.* **2012**, *51* (31), 7812−7816.
(61) Wilkins, L. E.; Badi, N.; Du Prez, F.; Gibson, M. I. Double-Modified Glycopolymers from Thiolactones to Modulate Lectin Selectivity and Affinity. *ACS Macro Lett.* **2018**, *7* (12), 1498−1502.
(62) Wijesundera, S. A.; Liyanage, S. H.; Biswas, P.; Reuther, J. F.; Yan, M. Trehalose-Grafted Glycopolymer: Synthesis via the Staudinger Reaction and Capture of Mycobacteria. *Biomacromolecules* **2023**, *24* (1), 238−245.
(63) Kruger, A. G.; Brucks, S. D.; Yan, T.; Cárcarmo-Oyarce, G.; Wei, Y.; Wen, D. H.; Carvalho, D. R.; Hore, M. J. A.; Ribbeck, K.; Schrock, R. R.; Kiessling, L. L. Stereochemical Control Yields Mucin Mimetic Polymers. *ACS Cent. Sci.* **2021**, *7* (4), 624−630.
(64) Qin, Q.; Yin, Z.; Wu, X.; Haas, K. M.; Huang, X. Valency and density matter: Deciphering impacts of immunogen structures on immune responses against a tumor associated carbohydrate antigen using synthetic glycopolymers. *Biomaterials* **2016**, *101*, 189−198.
(65) Joshi, S. Y.; Deshmukh, S. A. A review of advancements in coarse-grained molecular dynamics simulations. *Mol. Simul.* **2021**, *47* (10−11), 786−803.
(66) Mohammadi, E.; Joshi, S. Y.; Deshmukh, S. A. A review of computational studies of bottlebrush polymers. *Comput. Mater. Sci.* **2021**, *199*, No. 110720.
(67) Conway, O.; An, Y.; Bejagam, K. K.; Deshmukh, S. A. Development of transferable coarse-grained models of amino acids. *Mol. Syst. Des. Eng.* **2020**, *5* (3), 675−685.
(68) Mohammadi, E.; Joshi, S. Y.; Deshmukh, S. A. Development, Validation, and Applications of Nonbonded Interaction Parameters between Coarse-Grained Amino Acid and Water Models. *Biomacromolecules* **2023**, *24* (9), 4078−4092.
(69) An, Y.; Bejagam, K. K.; Deshmukh, S. A. Development of New Transferable Coarse-Grained Models of Hydrocarbons. *J. Phys. Chem. B* **2018**, *122* (28), 7143−7153.
(70) An, Y.; Bejagam, K. K.; Deshmukh, S. A. Development of Transferable Nonbonded Interactions between Coarse-Grained Hydrocarbon and Water Models. *J. Phys. Chem. B* **2019**, *123* (4), 909−921.
(71) Phillips, J. C.; Braun, R.; Wang, W.; Gumbart, J.; Tajkhorshid, E.; Villa, E.; Chipot, C.; Skeel, R. D.; Kalé, L.; Schulten, K. Scalable molecular dynamics with NAMD. *J. Comput. Chem.* **2005**, *26* (16), 1781−1802.
(72) Hsiao, P.-Y. Chain Morphology, Swelling Exponent, Persistence Length, Like-Charge Attraction, and Charge Distribution around a Chain in Polyelectrolyte Solutions: Effects of Salt Concentration and Ion Size Studied by Molecular Dynamics Simulations. *Macromolecules* **2006**, *39* (20), 7125−7137.
(73) Nygaard, M.; Kragelund, B. B.; Papaleo, E.; Lindorff-Larsen, K. An Efficient Method for Estimating the Hydrodynamic Radius of Disordered Protein Conformations. *Biophys. J.* **2017**, *113* (3), 550−557.
(74) Kadirvelraj, R.; Foley, B. L.; Dyekjaer, J. D.; Woods, R. J. Involvement of water in carbohydrate-protein binding: concanavalin A revisited. *J. Am. Chem. Soc.* **2008**, *130* (50), 16933−16942.
(75) Dalotto-Moreno, T.; Croci, D. O.; Cerliani, J. P.; Martinez-Allo, V. C.; Dergan-Dylon, S.; Méndez-Huergo, S. P.; Stupirski, J. C.; Mazal, D.; Osinaga, E.; Toscano, M. A.; Sundblad, V.; Rabinovich, G. A.; Salatino, M. Targeting Galectin-1 Overcomes Breast Cancer-Associated Immunosuppression and Prevents Metastatic Disease. *Cancer Res.* **2013**, *73* (3), 1107−1117.
(76) Lu, D.; Zhou, H.; Li, N.; Wang, Y.; Zhang, T.; Wang, F.; Liu, N.; Zhu, H.; Zhang, J.; Yang, Z.; Liu, Z. Galectin expression detected by 68Ga-galectracer PET as a predictive biomarker of radiotherapy resistance. *Eur. J. Nucl. Med. Mol. Imaging* **2022**, *49* (8), 2746−2760.
(77) Lerévérend, C.; Kotaich, N.; Cartier, L.; De Boni, M.; Lahire, S.; Fichel, C.; Thiebault, C.; Brabencova, E.; Maquin, C.; Barbosa, E.; Corsois, L.; Hotton, J.; Guendouzen, S.; Guilbert, P.; Lepagnol-Bestel, A.-M.; Cahen-Doidy, L.; Lehmann-Che, J.; Devy, J.; Bensussan, A.; Le Jan, S.; Pommier, A.; Merrouche, Y.; Le Naour, R.; Vignot, S.; Potteaux, S. Enhanced expression of galectin-9 in triple negative breast cancer cells following radiotherapy: Implications for targeted therapy. *Int. J. Cancer* **2024**, 1−14.
(78) Holden, H. M.; Rayment, I.; Thoden, J. B. Structure and Function of Enzymes of the Leloir Pathway for Galactose Metabolism*. *J. Biol. Chem.* **2003**, *278* (45), 43885−43888.
(79) Gestwicki, J. E.; Cairo, C. W.; Strong, L. E.; Oetjen, K. A.; Kiessling, L. L. Influencing Receptor−Ligand Binding Mechanisms with Multivalent Ligand Architecture. *J. Am. Chem. Soc.* **2002**, *124* (50), 14922−14933.
(80) Dam, T. K.; Roy, R.; Pagé, D.; Brewer, C. F. Negative Cooperativity Associated with Binding of Multivalent Carbohydrates to Lectins. Thermodynamic Analysis of the "Multivalency Effect. *Biochemistry* **2002**, *41* (4), 1351−1358.
(81) Restuccia, A.; Hudalla, G. A. Tuning carbohydrate density enhances protein binding and inhibition by glycosylated β-sheet peptide nanofibers. *Biomater. Sci.* **2018**, *6* (9), 2327−2335.

https://doi.org/10.1021/acs.biomac.4c01245
Biomacromolecules 2024, 25, 7985−7994